www.acsnano.org

Giant Enhancement of Four-Wave Mixing by Doubly Zone-Folded Nonlocal Metasurfaces

Stephanie C. Malek, Tenzin Norden, Chloe F. Doiron, Tomás Santiago-Cruz, Jaeyeon Yu, Alexander Cerjan, Prashant Padmanabhan, and Igal Brener*



ACCESS I Article Recommendations III Metrics & More Supporting Information Four-Wave Mixing **Four-Wave Mixing Intensity** $(2\omega_1 - \omega_2)$ Silicon-Rich Nitride Metasurface 0.5 Si Film on Glass (100x) -0.60 0.6 time delay (ps)

ABSTRACT: Resonant optical metasurfaces hold promise for enhancing nonlinear optical signals and manipulating their fundamental properties. However, they rarely excel at amplifying signals from nonlinear processes with two incident pump beams, such as four-wave mixing (FWM) or sum-frequency generation. Frequency-mixing experiments impose challenging requirements for metasurface design due to the need to support multiple optical resonances with compatible field profiles at specified resonant wavelengths, often across a substantial spectral separation. In this work, we introduce nonlocal 'quadromer' metasurfaces containing four nanostructures per unit cell as the key to unlocking configurable, multiresonant metasurfaces that enhance frequency-mixing processes. As a proof of concept, we experimentally demonstrate enhanced FWM using quadromer metasurfaces made of silicon and silicon-rich silicon nitride. The results are relevant for applications such as imaging of infrared light upconverted into the visible spectrum and the generation of quantum light via spontaneous FWM.

KEYWORDS: four-wave mixing, metamaterial, photonic crystal, quasi-bound state in the continuum, nonlinear metasurface, symmetry

INTRODUCTION

Downloaded via SANDIA NATL LABORATORIES on October 14, 2025 at 15:48:37 (UTC). See https://pubs.acs.org/sharingguidelines for options on how to legitimately share published articles.

Free-space metasurfaces supporting optical resonances have emerged as promising platforms for amplifying and controlling nonlinear optical signals. Optically thin resonant metasurfaces are advantageous because they enhance the local density of states (LDOS) and, therefore, the nonlinear signal while being unencumbered by phase-matching considerations. Early demonstrations of nonlinear dielectric metasurfaces used spectrally broadband optical modes, such as Mie modes, to resonantly enhance nonlinear signal generation. Recently, spectrally narrowband quasi-bound states in the continuum (q-BICs)⁴⁻⁷ have become a leading approach to enhance nonlinear optical processes due to their strong field enhancement and ability to tailor the field overlap with the nonlinear material. In the context of metasurfaces, q-BICs are typically supported by a periodic array of nanostructures with periodic

symmetry perturbations that allow a bound mode to leak into free space. A distinguishing characteristic of q-BICs is their engineerability, as their optical lifetimes (and thus, Q-factors) are controlled largely by the strength of the symmetry-breaking perturbation^{8,9} and their field distributions are determined by which symmetries are broken.¹⁰ Concurrent with higher Q-factors, metasurfaces supporting q-BICs enhance the LDOS and fields concentrated inside the active material and therefore consistently demonstrate strong enhancement of second^{7,11–14}

Received: June 26, 2025
Revised: September 18, 2025
Accepted: September 19, 2025

Published: September 29, 2025





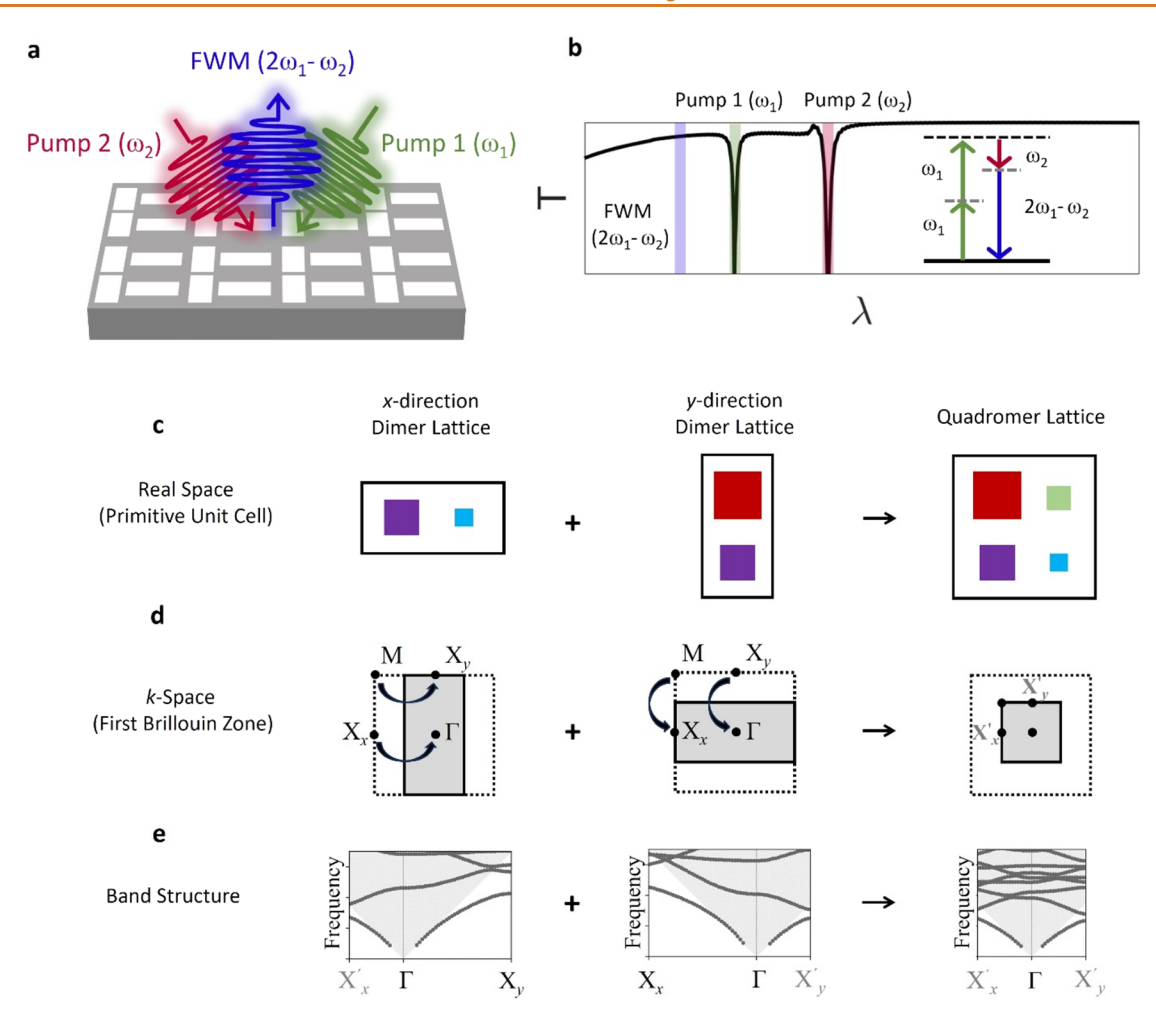


Figure 1. Illustration of doubly zone-folded metasurfaces for four-wave mixing by quadromer lattices. (a) Schematic of a metasurface supporting four-wave mixing with two incident pump beams. (b) Representative metasurface spectrum with resonances at the wavelength of each pump beam. (c-e) Conceptualization of doubly zone-folded quadromer lattices formed by combining two dimer lattices. (c, d) Schematics of x-dimerized, y-dimerized, and quadromerized lattices in (c) real space and (d) k-space with FBZ indicated in gray. (e) Band structures of x-dimerized, y-dimerized, and quadromerized lattices.

and third¹⁵⁻¹⁷ harmonic generation, high-harmonic generation, ¹⁸⁻²⁰ and quantum nonlinear processes such as spontaneous parametric down-conversion. ²¹

Despite substantial progress in enhancing harmonic generation, nonlinear processes with multiple pump beams remain challenging for high-Q dielectric metasurfaces. Metasurfaces with only one spectrally narrowband resonance²² or two broadband Mie modes² or plasmonic modes^{23,24} have enhanced frequency-mixing processes, a pathway to further improvement is enhancing the LDOS with moderately high-Q resonances at multiple relevant wavelengths, for example, at each pump beam. Crucially, these multiple resonances must have compatible field profiles following the nonlinear polarization of the selected nonlinear process and material. Typical metasurfaces cannot readily support multiple resonances with the appropriate field distributions and resonant wavelengths for multipump nonlinear experiments. Occasionally, metasurfaces with fine-tuned nanostructure dimensions have enhanced sum-frequency generation (SFG) or four-wave mixing (FWM) using an arbitrary pair of q-BICs²⁵⁻²⁷ or low Q-factor Mie modes² with little choice of field profiles and resonant wavelengths. As an alternative, recent demonstrations of doubly resonant metasurfaces for two-beam experiments

have relied on guided mode resonances²⁸ or using one q-BIC and one mode of another kind such as a Mie mode²⁹ or a guided mode resonance.³⁰ While inverse design³¹ and leveraging three q-BICs³² have both been proposed as methods to enhance frequency mixing, nanofabrication constraints may impede their successful experimental demonstration. In short, strong enhancement of frequency mixing in metasurfaces requires the development of robust and fabricable devices with tailorable narrowband optical resonances.

In this work, we demonstrate 3 orders of magnitude enhancement of four-wave mixing in doubly resonant nonlocal metasurfaces. Specifically, we introduce a rational design scheme based on symmetry to generate metasurfaces with deliberate q-BICs for each of the two pumps while retaining the flexibility to choose the wavelengths of the pumps and the upconverted nonlinear signal. To do so, we consider nonlocal metasurfaces made from 'quadromer' lattices with four nanostructures per unit cell that enable multiple q-BICs with deliberately selected fundamental properties. Nearly all previous metasurfaces supported q-BICs with periodic monomer (one nanostructure per unit cell) or dimer (two nanostructures per unit cell) lattices. We recently introduced quadromer lattices and validated their distinctive flexibility for

choosing the mode profiles of multiple q-BICs as well as their spectral separation.³³ Here, we experimentally demonstrate markedly enhanced FWM in both silicon and silicon-rich silicon nitride (SRN) metasurfaces by devising quadromer lattices that support q-BICs at two chosen pump wavelengths with suitable field profiles. The results validate a design approach that is broadly generalizable to other materials and a frequency-mixing process, which is promising for applications in quantum nonlinear processes and upconverted nonlinear imaging.

RESULTS

We first construct doubly resonant metasurfaces for FWM. The metasurfaces support resonances at the wavelengths of the two near-infrared (NIR) pumps (ω_1 and ω_2) to enhance a FWM process that upconverts the NIR frequencies into a visible nonlinear output with frequency $\omega_3 = 2\omega_1 - \omega_2$ (Figure 1a,b). We consider nonlocal metasurfaces with spatially extended optical modes whose resonant frequencies are dispersive in k-space such that the modes have a photonic band structure. Most nonlocal metasurfaces support q-BICs in periodic monomer or dimer lattices through symmetry-breaking perturbations.^{8,10} Dimerizing perturbations double the period along one direction in real space (Figure 1c, left and center panels) and correspondingly halve the period along the corresponding direction in k-space, which folds the photonic bands from the edge of the First Brillouin Zone (FBZ) (either the X or M high-symmetry point) to the Γ point at the center of the FBZ (Figure 1d, left and center panels). In doing so, the dimerizing perturbations take bound modes from under the light line at the edge of the FBZ (Figure 1e, left and center panels) and convert selected modes into radiative q-BICs that are excitable from free space at normal incidence.8 The symmetry of the dimer lattice determines which of the folded modes become radiative q-BICs and which polarization of freespace light excites each q-BIC. 10 Additionally, the strength of each symmetry-breaking perturbation partially controls the Qfactor of the corresponding q-BICs, such that Q is inversely proportional to the perturbation strength squared.8 Dimer lattices have emerged as a predominant method for supporting q-BICs but offer a limited selection of mode profiles and minimal ability to control the spectral separation between modes. We have recently demonstrated that a larger selection of BICs and q-BICs is achievable by dimerizing a lattice in two different in-plane directions, as any combination of two such folding operations from the M, X_x , or X_y points brings modes from all three high-symmetry points to Γ . Doubly folded lattices take the form of symmetry-broken quadromer lattices with four nanostructures per primitive unit cell (ex., Figure 1c, right panel). As with dimer lattices, the symmetry of the quadromer lattice determines which modes become radiative q-BICs, and the strength of the relevant symmetry-breaking perturbation controls their Q-factors.³³ Because the relationships between lattice symmetry and allowed q-BICs are known for dimer lattices, 10' an intuitive method to construct quadromer lattices is to combine two lattices that are dimerized along different directions so that the resulting quadromer inherits, at a minimum, the q-BICs folded by both dimerizing perturbations.³³ Figure 1c-e illustrates a simple quadromer with doubly folded bands formed by combining lattices dimerized in the x- and y- directions. In this example, both dimerizing perturbations make the two nanostructures of the dimer into different sizes (Figure 1c) and, in doing so, fold

the bands to Γ from an X point of the unperturbed lattice (Figure 1d,e).

Next, we selected a quadromer lattice that supports two q-BICs with suitable mode profiles to enhance FWM when the q-BICs are excited by two incident pump beams. On a platform of apertures etched into a thin film of amorphous silicon, we formulate a quadromer lattice by combining an xdimerized lattice with a y-dimerized lattice such that each dimer supports a q-BIC for a pump beam. With many choices for combinations of q-BIC mode profiles, we consider the nonlinear polarization for four-wave mixing for guidance. For Pump 1 at ω_1 and Pump 2 at ω_2 the nonlinear polarization is $P(2\hat{\omega}_1 - \omega_2) = 9\varepsilon_0 \chi^{(3)}[E(\omega_1)E^*(\omega_2)E(\omega_1)]$ when nonzero $\chi^{(3)}$ tensor components are set equal to approximate amorphous or polycrystalline silicon. The nonlinear polarization indicates that for an optimal nonlinear interaction, the q-BICs at both pumps need spatially overlapping profiles with electric field components along at least one of the same Cartesian directions. Figure 2a illustrates the construction of a

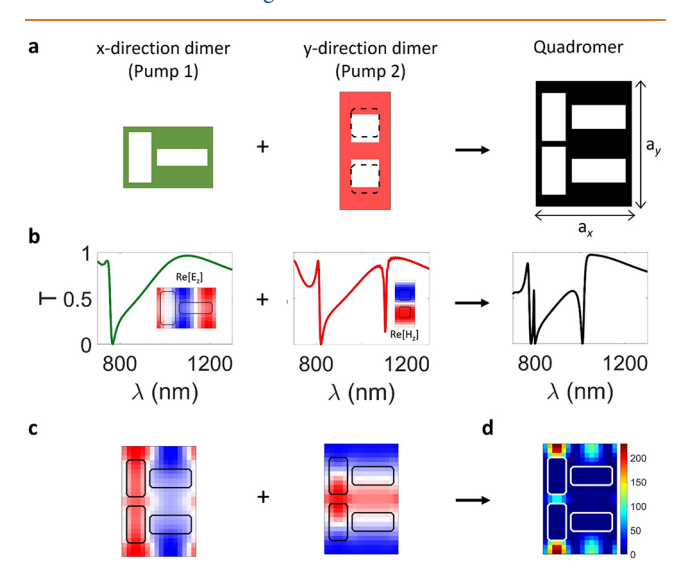


Figure 2. Construction of a quadromer lattice for four-wave mixing from two dimer lattices. (a) Schematic of selected dimer lattices and their combined quadromer lattice. The white area indicates apertures etched into silicon. The dimerizing perturbation in the y-direction is a 'spacing' perturbation, where each nanostructure is closer to one of its neighbors. (b) Simulated spectra of dimer lattices and their combined quadromer lattice. Insets: Field profiles of dominant out-of-plane component (E_z for Pump 1 q-BIC, H_z for Pump 2 q-BIC). (c) E_x field component of constituent dimer lattices. (d) $|E_x(\omega_1)E_x^*(\omega_2)E_x(\omega_1)|$ in silicon in the quadromer lattice as a proxy for enhancement of four-wave mixing following the nonlinear polarization.

quadromer by combining an x-direction dimer and a y-direction dimer. In this particular quadromer, each constituent dimer conforms to the p2mm crystallographic wallpaper group, but with the nanostructures positioned differently with respect to the mirror planes. The x-dimerized lattice supports an 'antibonding' q-BIC folded from X_x (for Pump 1) with the electric field as the dominant field component in the propagation direction (TM), and the y-dimerized lattice folds a 'bonding' TE q-BIC from X_y (for Pump 2) (Figure 2b). The simulated spectrum of the quadromer is predominantly the combined spectrum of both dimers, such that the quadromer supports the selected q-BICs from each dimer. Both modes

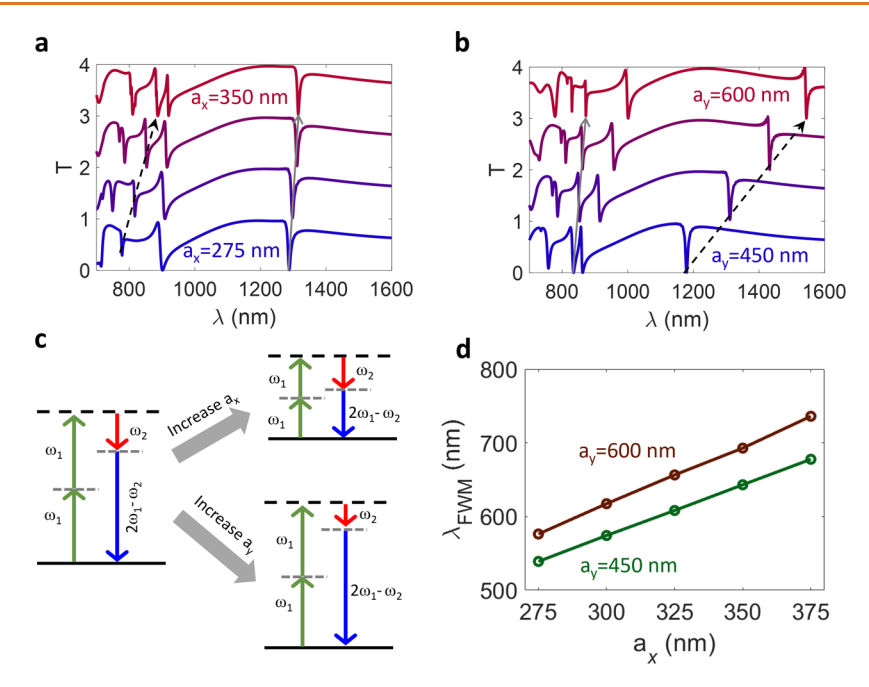


Figure 3. Selection of resonant wavelengths via tuning of the quadromer lattice constant. (a, b) Simulated transmission spectra as a function of (a) a_x and (b) a_y . (c) Illustration of the enhanced four-wave mixing process and its wavelength dependencies on a_x and a_y . (d) Four-wave mixing wavelength as a function of lattice constant when the metasurface is pumped at the two selected q-BICs.

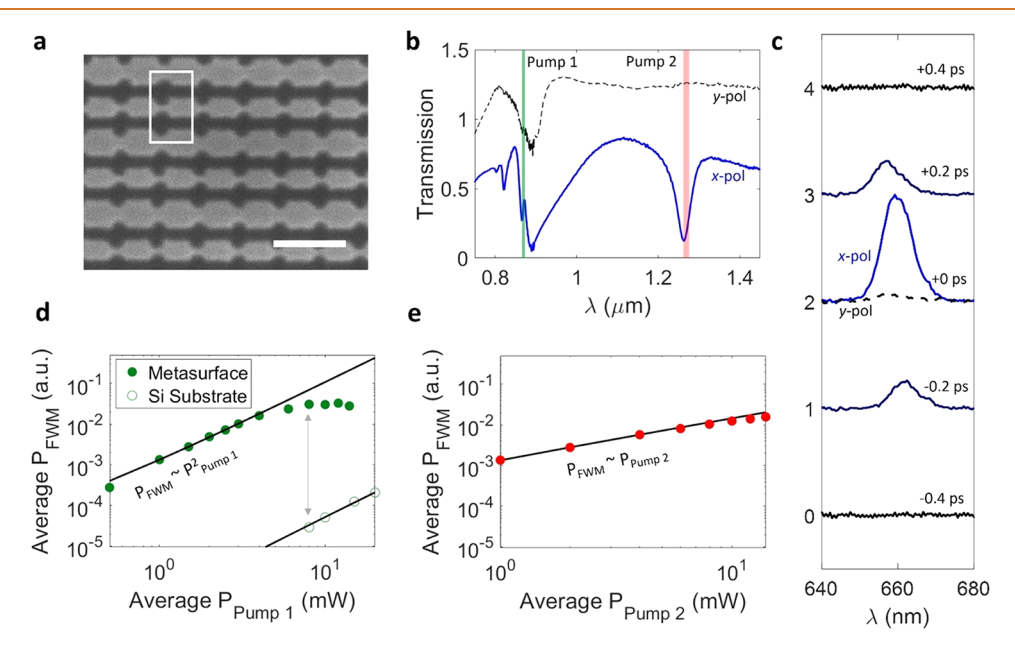


Figure 4. Experimental demonstration of enhanced four-wave mixing in a silicon quadromer metasurface. (a) Scanning electron micrograph of a fabricated device with lattice constants $a_x = 285$ nm and $a_y = 500$ nm, and y-direction spacing perturbation $d_Y = 26$ nm. Scale bar: 500 nm. The white box indicates one unit cell. (b) Measured linear transmission spectrum for x-polarized (blue curve) and y-polarized (dashed black curve) white light, with y-polarized spectrum offset by 0.5. Green and red shaded areas indicate the wavelength and bandwidth of Pump 1 and Pump 2, respectively. (c) Measured FWM spectra as a function of time delay between the two pump beams. Pumps are x-polarized except for the dashed black line. The dashed black line represents measured FWM when incident pump beams are both y-polarized. Spectra artificially offset by 1. (d, e) Measured FWM power as a function of (d) Pump 1 and (e) Pump 2 power with the other pump power held constant at 2 mW.

have an appreciable x-component of their electric fields (Figure 2c) and considerable spatial overlap with each other following the nonlinear polarizations (E_x component in Figure 2d, E_y and E_z components, and nonresonantly excited E_x component in Figure S1). Additionally, as the perturbation strength of each constituent dimer is the primary factor controlling the Q-factor of its own q-BIC, 33 the Q-factors and field enhancement are

readily tunable (Figure S2). While quadromers can be configured to support many different combinations of q-BICs,³³ we choose one TE mode and one TM mode to introduce a larger spectral separation between the modes. In the selected quadromer lattice, both q-BICs are excited by *x*-polarized incident light. However, rotating the apertures by 45°

would allow the Pump 1 q-BIC to be excited instead by *y*-polarized free-space light if desired.^{33,34}

In quadromers composed of x- and y-direction dimers, the spectral separation between q-BICs is readily configurable, which allows the metasurface to conform to specified pump wavelengths or generate four-wave mixing at a desired wavelength. Expanding (contracting) the lattice along the xdirection red-shifts (blue-shifts) the q-BIC for Pump 1 that was folded from X_x with minimal impact to the resonant wavelength of the q-BIC for Pump 2 (Figure 3a). Similarly, expanding or contracting the lattice along the y-direction primarily controls the resonant wavelength of Pump 2 without significantly shifting the Pump 1 resonance (Figure 3b). As such, the quadromer lattice can be readily adapted to accommodate pump beams at a range of NIR wavelengths and to choose the wavelength of enhanced FWM (Figure 3c). In this example, changing the x-direction lattice constant (a_x) from 450 to 600 nm red-shifts the Pump 1 q-BIC by more than 350 nm while only red-shifting the Pump 2 q-BIC by less than 40 nm. Consequently, the lattice can be configured to support enhanced FWM signal within a broad choice of wavelengths (i.e., half of the visible spectrum) even before any fine-tuning or optimization and without compromising the choice of mode profiles (Figure 3d). Such flexibility is not attainable in dimer lattices and is instead only possible because the two relevant q-BICs are folded to Γ from different high-symmetry points.

We experimentally demonstrate enhancement of the FWM process using our proposed formalism on a silicon metasurface. Using standard cleanroom processes, we fabricate a metasurface in \sim 200 nm thick amorphous silicon on glass (Figure 4a), selecting lattice constants that make the metasurface compatible with our laser systems. Linear measurements show that the fabricated metasurface supports the designed q-BICs at 865 nm for Pump 1 and at 1260 nm for Pump 2. The metasurface supports the designed q-BICs with substantial field overlap, despite the nanofabrication imperfection that merges adjacent structures (Figure S3). The strength of the symmetry perturbation in each dimer controls the Q-factor of its respective q-BIC, resulting in Q-factors of ~130 for Pump 1 and \sim 20 for Pump 2 when illuminated by x-polarized light (Figure 4b). To measure FWM, we excite the metasurface with two pulsed femtosecond laser beams such that each incident beam is resonant with one q-BIC and both beams are spatially and temporally overlapped. Figure 4c shows the measured FWM signal centered at around 650 nm and its dependence on the temporal overlap of the two pump beams. Pumping the metasurface with y-polarized pump beams to avoid exciting the q-BICs results in minimal enhancement of four-wave mixing (dashed curve in Figure 4c), which is consistent with calculations (Figure S2). We further validate that the upconverted signal originates from the FWM because its intensity varies quadratically with the power of Pump 1 (Figure 4d) but linearly with the power of Pump 2 (Figure 4e). Additional polarization- and wavelength-dependent measurements corroborate that enhancement of FWM is a resonant effect, dependent on the excitation of the designed pair of q-BIC (Figure S4). We estimate that, relative to the unpatterned thin film, the metasurface enhances FWM by a factor of at least ~1040 (Figure 4d at 8 mW average Pump 1 power, gray arrow), which is nearly double the enhancement previously demonstrated with two arbitrarily selected q-BICs.²⁵ The metasurface likely enhances FWM by a factor of more than 2000 because (1) the FWM signal on the metasurface saturates

as a function of power at high pump power but the substrate exhibits a poor signal-to-noise ratio at low power, and (2) we measured ~2400x enhancement measured at a different spot on the device due to the effects of local variances in nanofabrication (Figure S5). The measurements are further prone to underestimating the enhancement relative to the unpatterned thin film because they are conducted in a reflection geometry where we pump the metasurface and collect the nonlinear signal through the same objective. The numerical aperture (NA) of the objective is 0.4, which is a higher-than-ideal NA for exciting the q-BICs with angular dispersion (Figure S6) but also too low to collect a nonlinear signal from all of the diffracted orders of the metasurface (whereas an unpatterned thin film lacks higher-than-zero order diffraction). We note that more accurate fabrication and higher Q-factors do not automatically improve experimentally measured frequency-mixing enhancement (Figure S7), especially if the spectrally narrowband resonances cannot make use of the entire bandwidth of the pulsed pump beams.

While enhancing the LDOS with q-BICs improves FWM, it also causes the metasurface to struggle under high-power excitation. The metasurface demonstrates saturation of the nonlinear signal at a high pump power (Figure 4d). Saturation of four-wave mixing in silicon devices is a known phenomenon for both photonic integrated circuits and metasurfaces. ^{22,35–41} The physical origins of intensity-dependent saturation are typically attributed to two-photon absorption (TPA) and freecarrier absorption, and nanophotonic devices that introduce field enhancement and confinement increase two-photon absorption and lower the saturation threshold. 42,43 Under high-power illumination from Pump 1 (average power >4 mW or peak power density $> \sim 23 \text{ GW/cm}^2$), the FWM signal from the metasurface, but not the unpatterned thin film, saturates as a function of pump power (Figure 4d), which is suggestive of resonant enhancement of TPA at a comparable level to previous silicon metasurfaces.³⁹ Additionally, when Pump 2 is y-polarized and therefore nonresonant, the threshold for saturation increases by approximately a factor of 3 (Figure S8), indicating that both q-BICs contribute to resonant enhancement of the nonlinear absorption. TPA enhancement in metasurfaces depends partially on Q-factor, 42 as higher Q resonances tend to introduce larger LDOS enhancement. A pathway to minimizing or even preventing TPA while leveraging q-BICs with moderate-to-high Q-factors is increasing the bandgap of the material. Previously, silicon-rich silicon nitride (SRN) has been used in integrated photonics to reduce two-photon absorption in four-wave mixing because it has a wider bandgap than silicon. 40,41 SRN is typically grown by plasma enhanced chemical vapor deposition (PECVD), such that the ratio of precursor gases can be adjusted to tailor the optical properties nearly between those of silicon and silicon nitride. 44 Increasing the silicon concentration of silicon nitride increases its refractive index, 44 linear absorption, 44 and $\chi^{(3)}$ values.45

We develop doubly resonant metasurfaces made of siliconrich silicon nitride that enhance FWM with less TPA than silicon. As our design paradigm depends on symmetry rather than fine-tuning the nanostructure dimensions, it can be applied to different material platforms to support the same selected q-BICs, often without fundamental changes to the design. Indeed, by using a \sim 440 nm thick SRN film with a refractive index of $n \sim 3.3$ at $\lambda = 600$ nm, the required metaunit dimensions are even similar to those of the \sim 200 nm thick

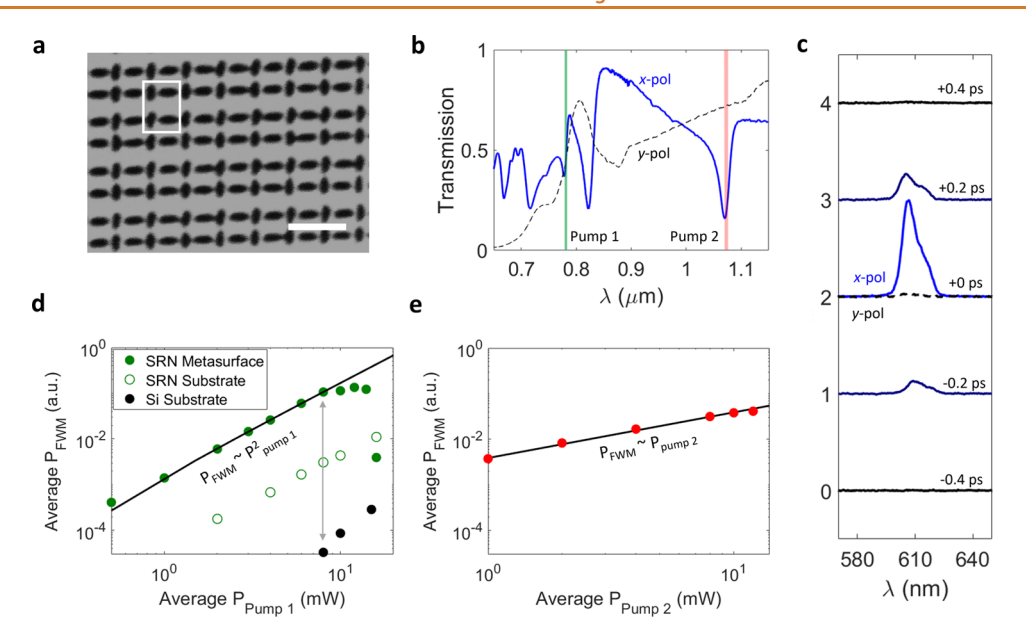


Figure 5. Experimental demonstration of enhanced FWM in a silicon-rich nitride quadromer metasurface. (a) Scanning electron micrograph of fabricated device with lattice constants $a_x = 315$ nm, and $a_y = 450$ nm and y-direction spacing perturbation $d_Y = 25$ nm. Scale bar: 500 nm. The white box indicates one unit cell. (b) Measured linear transmission spectrum for x-polarized (blue line) and y-polarized (black dashed line) light. The green and red shaded areas indicate the wavelength and bandwidth of Pump 1 and Pump 2, respectively. (c) Measured FWM spectra as a function of time delay between the two pump beams for x-polarized incident pump beams. Pumps are x-polarized except for the dashed black line. The dashed black line represents measured FWM when incident pump beams are both y-polarized. Spectra artificially offset by 1. (d, e) Measured FWM power as a function of (d) Pump 1 and (e) Pump 2 power with the other pump power held constant at 2 mW.

silicon metasurface (Figure S6). We fabricate SRN metasurfaces following the same protocol as that for the silicon metasurfaces. Figure 5a shows a fabricated SRN metasurface that supports q-BICs for Pump 1 at 777 nm with a $Q \sim 145$ and Pump 2 at 1070 nm with a $Q \sim 45$ (Figure 5b). The metasurface supports FWM centered at ~600 nm, with a clear dependence on the temporal overlap of the two pump beams and their polarizations (Figure 5c). As with the silicon metasurface, the FWM signal has a quadratic dependence on the power of Pump 1 (Figure 5d) and a linear dependence on the power of Pump 2 (Figure 5e). The SRN metasurface enhances FWM by a factor of approximately ~40 relative to the unpatterned SRN film on a glass substrate, and the lower field enhancement compared to the silicon metasurface is consistent with simulations (Figure S9). Compared to the unpatterned silicon thin film on a glass substrate used for the silicon metasurface in Figure 5, the SRN metasurface enhances FWM by a factor of ~3200 when pumped at the same wavelengths (at 8 mW average power, gray arrow in Figure 5c), partly because of the lower linear absorption in the SRN film at visible wavelengths (Figure S10). The metasurface barely exhibits an indication of enhanced TPA (Figure 5c). Admittedly, the device burns under very high-power excitation from Pump 1 (\sim 14 mW average power or \sim 79 GW/cm²), even though the silicon metasurface in Figure 4 does not show similar indications of damage (i.e., burn marks and decreased, not just saturated four-wave mixing). We note that the highpower performance of SRN metasurfaces may be improved by decreasing the silicon content to improve the damage threshold⁴⁵ or adopting thermal management strategies such as the use of a thermally conductive substrate. Overall, the SRN metasurface provides comparable enhancement to the silicon metasurface, while avoiding the strong two-photon absorption of silicon metasurfaces at high power.

CONCLUSIONS

In summary, we have experimentally demonstrated nonlocal metasurfaces that enhance FWM by more than 3 orders of magnitude. The considerable enhancement is generated by a rational design paradigm that uses periodic quadromer lattices to support appropriate q-BICs for two pump beams at deliberately chosen wavelengths and free-space polarizations. Our demonstration of FWM suggests, more generally, that symmetry-based design of quadromer lattices can improve nonlinear signal generation in multipump processes. The lattice (and therefore the selected pair of q-BICs) presented in this work represents just one option out of dozens of possible quadromer lattices and combinations of q-BICs. Indeed, we have previously shown that quadromer lattices can support several q-BICs with deliberately chosen properties.³³ In the context of multibeam nonlinear optical processes, triply or quadrupally resonant metasurfaces could dramatically enhance a nonlinear signal by introducing appropriate resonances not just at the pump wavelengths but also at the wavelengths of the generated nonlinear signals. We demonstrated that the design of quadromer lattices is readily generalizable to a variety of material platforms and scalable to most desired wavelength ranges because of its dependence on symmetry rather than precise fine-tuning of the nanostructure dimensions. We anticipate that rationally designed multiresonant metasurfaces for the frequency-mixing process will prove useful for nonlinear upconverted imaging^{22,2} and quantum nonlinear processes such as doubly resonant metasurfaces for nondegenerate spontaneous parametric down-conversion. 21,46,47 Moreover, our design paradigm opens the door for the demonstration of quantum third-order nonlinear processes such as spontaneous FWM (SFWM) and photon triplet generation via spontaneous parametric down-conversion that are yet to be

observed in metasurfaces. Our platform is readily applicable for SFWM, which has already been observed in unpatterned SRN films similar to the ones used in this work. 45

METHODS

Fabrication. The silicon device was fabricated on a \sim 200 nm thick silicon film grown by low-pressure chemical vapor deposition on a JGS2 fused silica substrate. The silicon-rich nitride device was fabricated on a \sim 440 nm thick film grown on JGS2 fused silica substrate by plasma-enhanced chemical vapor deposition with SiH₄ and N₂ precursor gases. The metasurfaces were patterned into ZEP520A resist with an anticharging layer (DisChem Inc.) by a 100 keV electron-beam lithography system after data preparation with BEAMER software (GenlSys GmbH). All metasurfaces were etched by a reactive ion etch process with SF₆ and C₄F₈ gases. The remaining ZEP resist was removed by a PG remover at 80 °C.

Linear Measurements. Linear transmission measurements were conducted in a home-built optical microscope with a white light source and separate Ocean Optics spectrometers for visible and near-infrared wavelengths. The numerical aperture of the lens for incident light is \sim 0.1. *Q*-factors are estimated as $Q \sim \text{fwhm}/\lambda_{\text{res}}$.

Nonlinear Measurements. Pump 1 was supplied by a Ti:sapphire oscillator (Chameleon Ultra II, Coherent), which produced ~140 fs pulses with an 80 MHz repetition rate. Pump 2 was generated by an optical parametric oscillator, pumped by the Ti:sapphire oscillator, capable of producing broadly tunable pulses spanning 1000-1600 nm. A 20× objective was used to focus the beams onto the sample to a beam spot size of $\sim 2 \mu m$. The beams were spatially and temporally overlapped on the sample to ensure efficient nonlinear interaction. The same objective was also used to collect the reflected signal, which was directed either to a spectrometer for spectral measurements or to a photomultiplier tube (PMT) (Hamamatsu R943-02) for power studies. A combination of a half-wave plate (HWP) and a polarizer was used to control the beam power during power-dependent measurements, while additional HWPs were used to control the linear polarization angle of the two pump beams. In both cases, a short pass filter (λ < 750 nm) and a bandpass filter (650 \pm 40 or 600 \pm 40 nm) were used to isolate the nonlinear signal on the detection side. Pump 2 was chopped at 1 kHz for phase-sensitive detection with a lock-in amplifier and PMT.

Électromagnetic Simulations. Lumerical FDTD was used to design the metasurfaces. Band structures were calculated in Legume using guided mode expansion. 48,49

ASSOCIATED CONTENT

Supporting Information

The Supporting Information is available free of charge at https://pubs.acs.org/doi/10.1021/acsnano.5c10747.

Additional measurements of metasurface in Figure S4, measurements of an additional silicon metasurface, and additional simulations of metasurfaces in Figures S4 and S5 (PDF)

AUTHOR INFORMATION

Corresponding Author

Igal Brener — Center for Integrated Nanotechnologies, Sandia National Laboratories, Albuquerque, New Mexico 87123, United States; orcid.org/0000-0002-2139-5182; Email: ibrener@sandia.gov

Authors

Stephanie C. Malek – Center for Integrated Nanotechnologies, Sandia National Laboratories, Albuquerque, New Mexico 87123, United States; Oorcid.org/0009-0006-1420-7231

- **Tenzin Norden** Center for Integrated Nanotechnologies, Los Alamos National Laboratory, Los Alamos, New Mexico 87545, United States; Orcid.org/0000-0002-7114-3768
- Chloe F. Doiron Center for Integrated Nanotechnologies, Sandia National Laboratories, Albuquerque, New Mexico 87123, United States
- Tomás Santiago-Cruz Center for Integrated Nanotechnologies, Sandia National Laboratories, Albuquerque, New Mexico 87123, United States
- Jaeyeon Yu Center for Integrated Nanotechnologies, Sandia National Laboratories, Albuquerque, New Mexico 87123, United States
- Alexander Cerjan Center for Integrated Nanotechnologies, Sandia National Laboratories, Albuquerque, New Mexico 87123, United States; oorcid.org/0000-0002-4362-7300
- Prashant Padmanabhan Center for Integrated Nanotechnologies, Los Alamos National Laboratory, Los Alamos, New Mexico 87545, United States; orcid.org/ 0000-0002-1881-5262

Complete contact information is available at: https://pubs.acs.org/10.1021/acsnano.5c10747

Notes

The authors declare no competing financial interest.

ACKNOWLEDGMENTS

This work was supported by the U.S. Department of Energy, Office of Basic Energy Sciences, Division of Materials Sciences and Engineering under Field Work Proposal Number 24-017574 and performed, in part, at the Center for Integrated Nanotechnologies, an Office of Science User Facility operated for the U.S. Department of Energy (DOE) Office of Science. Sandia National Laboratories is a multimission laboratory managed and operated by National Technology and Engineering Solutions of Sandia, LLC, a wholly owned subsidiary of Honeywell International, Inc., for the U.S. Department of Energy's National Nuclear Security Administration under contract DE-NA0003525. This paper describes objective technical results and analysis. Any subjective views or opinions that might be expressed in the paper do not necessarily represent the views of the U.S. Department of Energy or the United States Government.

REFERENCES

- (1) Liu, S.; Sinclair, M. B.; Saravi, S.; Keeler, G. A.; Yang, Y.; Reno, J.; Peake, G. M.; Setzpfandt, F.; Staude, I.; Pertsch, T.; Brener, I. Resonantly Enhanced Second-Harmonic Generation Using III–V Semiconductor All-Dielectric Metasurfaces. *Nano Lett.* **2016**, *16* (9), 5426–5432.
- (2) Liu, S.; Vabishchevich, P. P.; Vaskin, A.; Reno, J. L.; Keeler, G. A.; Sinclair, M. B.; Staude, I.; Brener, I. An All-Dielectric Metasurface as a Broadband Optical Frequency Mixer. *Nat. Commun.* **2018**, *9* (1), No. 2507.
- (3) Camacho-Morales, R.; Rahmani, M.; Kruk, S.; Wang, L.; Xu, L.; Smirnova, D. A.; Solntsev, A. S.; Miroshnichenko, A.; Tan, H. H.; Karouta, F.; Naureen, S.; Vora, K.; Carletti, L.; De Angelis, C.; Jagadish, C.; Kivshar, Y. S.; Neshev, D. N. Nonlinear Generation of Vector Beams From AlGaAs Nanoantennas. *Nano Lett.* **2016**, *16* (11), 7191–7197.
- (4) Hsu, C. W.; Zhen, B.; Lee, J.; Chua, S.-L.; Johnson, S. G.; Joannopoulos, J. D.; Soljačić, M. Observation of Trapped Light within the Radiation Continuum. *Nature* **2013**, 499 (7457), 188–191.

- (5) Plotnik, Y.; Peleg, O.; Dreisow, F.; Heinrich, M.; Nolte, S.; Szameit, A.; Segev, M. Experimental Observation of Optical Bound States in the Continuum. *Phys. Rev. Lett.* **2011**, *107* (18), No. 183901.
- (6) Campione, S.; Liu, S.; Basilio, L. I.; Warne, L. K.; Langston, W. L.; Luk, T. S.; Wendt, J. R.; Reno, J. L.; Keeler, G. A.; Brener, I.; Sinclair, M. B. Broken Symmetry Dielectric Resonators for High Quality Factor Fano Metasurfaces. *ACS Photonics* **2016**, 3 (12), 2362–2367.
- (7) Vabishchevich, P. P.; Liu, S.; Sinclair, M. B.; Keeler, G. A.; Peake, G. M.; Brener, I. Enhanced Second-Harmonic Generation Using Broken Symmetry III–V Semiconductor Fano Metasurfaces. *ACS Photonics* **2018**, *5* (5), 1685–1690.
- (8) Koshelev, K.; Lepeshov, S.; Liu, M.; Bogdanov, A.; Kivshar, Y. Asymmetric Metasurfaces with High-Q Resonances Governed by Bound States in the Continuum. *Phys. Rev. Lett.* **2018**, *121* (19), No. 193903.
- (9) Overvig, A. C.; Shrestha, S.; Yu, N. Dimerized High Contrast Gratings. *Nanophotonics* **2018**, *7* (6), 1157–1168.
- (10) Overvig, A. C.; Malek, S. C.; Carter, M. J.; Shrestha, S.; Yu, N. Selection Rules for Quasibound States in the Continuum. *Phys. Rev. B* **2020**, *102* (3), No. 035434.
- (11) Bernhardt, N.; Koshelev, K.; White, S. J. U.; Meng, K. W. C.; Fröch, J. E.; Kim, S.; Tran, T. T.; Choi, D.-Y.; Kivshar, Y.; Solntsev, A. S. Quasi-BIC Resonant Enhancement of Second-Harmonic Generation in WS2Monolayers. *Nano Lett.* **2020**, *20* (7), 5309–5314.
- (12) Anthur, A. P.; Zhang, H.; Paniagua-Dominguez, R.; Kalashnikov, D. A.; Ha, S. T.; Maß, T. W. W.; Kuznetsov, A. I.; Krivitsky, L. Continuous Wave Second Harmonic Generation Enabled by Quasi-Bound-States in the Continuum on Gallium Phosphide Metasurfaces. *Nano Lett.* **2020**, *20* (12), 8745–8751.
- (13) Fan, K.; Chen, H.; Sergeev, A. A.; Xing, Z.; Zhu, R.; Lau, K. M.; Wu, L.; Wong, K. S. Efficient Second-Harmonic Generation with Weak Polarization Sensitivity in Gallium Nitride Metasurfaces via Bound States in the Continuum. *Adv. Opt. Mater.* **2024**, *12* (23), No. 2400815.
- (14) Liu, Z.; Wang, J.; Chen, B.; Wei, Y.; Liu, W.; Liu, J. Giant Enhancement of Continuous Wave Second Harmonic Generation from Few-Layer GaSe Coupled to High-Q Quasi Bound States in the Continuum. *Nano Lett.* **2021**, *21* (17), 7405–7410.
- (15) Liu, Z.; Xu, Y.; Lin, Y.; Xiang, J.; Feng, T.; Cao, Q.; Li, J.; Lan, S.; Liu, J. High-Q Quasibound States in the Continuum for Nonlinear Metasurfaces. *Phys. Rev. Lett.* **2019**, *123* (25), No. 253901.
- (16) Hsiao, H.-H.; Hsieh, J.-C.; Liu, A.-Y.; Lin, K.-I.; Hsu, Y.-C. Enhancement of Third-Harmonic Generation in All-Dielectric Kite-Shaped Metasurfaces Driven by Quasi-Bound States in the Continuum. *Nanophotonics* **2024**, *13* (17), 3155–3164.
- (17) Liu, T.; Qin, M.; Qiu, J.; Tu, X.; Qiu, H.; Wu, F.; Yu, T.; Liu, Q.; Xiao, S. Polarization-Independent Enhancement of Third-Harmonic Generation Empowered by Doubly Degenerate Quasi-Bound States in the Continuum. *Nano Lett.* **2025**, *25*, 3646–3652.
- (18) Ginsberg, J. S.; Overvig, A. C.; Jadidi, M. M.; Malek, S. C.; Patwardhan, G. N.; Swenson, N.; Yu, N.; Gaeta, A. L. Enhanced Harmonic Generation in Gases Using an All-Dielectric Metasurface. *Nanophotonics* **2020**, *10* (1), 733–740.
- (19) Zograf, G.; Koshelev, K.; Zalogina, A.; Korolev, V.; Hollinger, R.; Choi, D.-Y.; Zuerch, M.; Spielmann, C.; Luther-Davies, B.; Kartashov, D.; Makarov, S. V.; Kruk, S. S.; Kivshar, Y. High-Harmonic Generation from Resonant Dielectric Metasurfaces Empowered by Bound States in the Continuum. *ACS Photonics* **2022**, *9* (2), 567–574.
- (20) Liu, H.; Guo, C.; Vampa, G.; Zhang, J. L.; Sarmiento, T.; Xiao, M.; Bucksbaum, P. H.; Vučković, J.; Fan, S.; Reis, D. A. Enhanced High-Harmonic Generation from an All-Dielectric Metasurface. *Nat. Phys.* **2018**, *14* (10), 1006–1010.
- (21) Santiago-Cruz, T.; Gennaro, S. D.; Mitrofanov, O.; Addamane, S.; Reno, J.; Brener, I.; Chekhova, M. V. Resonant Metasurfaces for Generating Complex Quantum States. *Science* **2022**, *377* (6609), 991–995.

- (22) Zheng, Z.; Smirnova, D.; Sanderson, G.; Cuifeng, Y.; Koutsogeorgis, D. C.; Huang, L.; Liu, Z.; Oulton, R.; Yousefi, A.; Miroshnichenko, A. E.; Neshev, D. N.; O'Neill, M.; Rahmani, M.; Xu, L. Broadband Infrared Imaging Governed by Guided-Mode Resonance in Dielectric Metasurfaces. *Light Sci. Appl.* **2024**, *13* (1), No. 249.
- (23) Wang, J.; Lv, B.; Liu, D.; Gong, W.; Shi, J. Efficient Four-Wave Mixing Based on Multiple Plasmonic Resonance. *Opt. Lett.* **2021**, *46* (18), 4522–4525.
- (24) Yang, J.; Xiao, X.; Flórez, J.; Gemmell, N.; Dichtl, P.; Gennaro, S. D.; Maier, S. A.; Phillips, C. C.; Clark, A. S.; Oulton, R. F. Stimulated Emission Tomography of Spontaneous Four-Wave Mixing in Plasmonic Nanoantennas. *ACS Photonics* **2025**, *12*, 4415–4422.
- (25) Moretti, G. Q.; Weber, T.; Possmayer, T.; Cortés, E.; de S Menezes, L.; Bragas, A. V.; Maier, S. A.; Tittl, A.; Grinblat, G. Si Metasurface Supporting Multiple Quasi-BICs for Degenerate Four-Wave Mixing. *Nanophotonics* **2024**, *13*, 3421–3428.
- (26) Camacho-Morales, R.; Xu, L.; Zhang, H.; Ha, S. T.; Krivitsky, L.; Kuznetsov, A. I.; Rahmani, M.; Neshev, D. Sum-Frequency Generation in High-Q GaP Metasurfaces Driven by Leaky-Wave Guided Modes. *Nano Lett.* **2022**, 22 (15), 6141–6148.
- (27) Feng, S.; Liu, T.; Chen, W.; Wu, F.; Xiao, S. Enhanced Sum-Frequency Generation from Etchless Lithium Niobate Empowered by Dual Quasi-Bound States in the Continuum. *Sci. China:Phys., Mech. Astron.* **2023**, *66* (12), No. 124214.
- (28) Molina, L. V.; Morales, R. C.; Zhang, J.; Schiek, R.; Staude, I.; Sukhorukov, A. A.; Neshev, D. N. Enhanced Infrared Vision by Nonlinear Up-Conversion in Nonlocal Metasurfaces. *Adv. Mater.* **2024**, *36* (31), No. 2402777.
- (29) Xu, L.; Smirnova, D. A.; Camacho-Morales, R.; Aoni, R. A.; Kamali, K. Z.; Cai, M.; Ying, C.; Zheng, Z.; Miroshnichenko, A. E.; Neshev, D. N.; Rahmani, M. Enhanced Four-Wave Mixing from Multi-Resonant Silicon Dimer-Hole Membrane Metasurfaces. *New J. Phys.* **2022**, 24 (3), No. 035002.
- (30) Qin, M.; Wu, F.; Liu, T.; Zhang, D.; Xiao, S. Enhanced Third-Harmonic Generation and Degenerate Four-Wave Mixing in an All-Dielectric Metasurface via Brillouin Zone Folding Induced Bound States in the Continuum. *Phys. Rev. B* **2025**, *111* (3), No. 035414.
- (31) Li, N.; Zhang, J.; Neshev, D. N.; Sukhorukov, A. A. Inverse Design of Nonlinear Metasurfaces for Sum Frequency Generation. *Nanophotonics* **2024**, *13*, 3363–3372.
- (32) Liu, T.; Qin, M.; Wu, F.; Xiao, S. High-Efficiency Optical Frequency Mixing in an All-Dielectric Metasurface Enabled by Multiple Bound States in the Continuum. *Phys. Rev. B* **2023**, *107* (7), No. 075441.
- (33) Malek, S. C.; Doiron, C. F.; Brener, I.; Cerjan, A. Robust Multiresonant Nonlocal Metasurfaces by Rational Design. *Nanophotonics* **2025**, *14*, 449–458.
- (34) Overvig, A. C.; Malek, S. C.; Yu, N. Multifunctional Nonlocal Metasurfaces. *Phys. Rev. Lett.* **2020**, *125* (1), No. 017402.
- (35) Corcoran, B.; Monat, C.; Grillet, C.; Moss, D. J.; Eggleton, B. J.; White, T. P.; O'Faolain, L.; Krauss, T. F. Green Light Emission in Silicon through Slow-Light Enhanced Third-Harmonic Generation in Photonic-Crystal Waveguides. *Nat. Photonics* **2009**, *3* (4), 206–210.
- (36) Shcherbakov, M. R.; Neshev, D. N.; Hopkins, B.; Shorokhov, A. S.; Staude, I.; Melik-Gaykazyan, E. V.; Decker, M.; Ezhov, A. A.; Miroshnichenko, A. E.; Brener, I.; Fedyanin, A. A.; Kivshar, Y. S. Enhanced Third-Harmonic Generation in Silicon Nanoparticles Driven by Magnetic Response. *Nano Lett.* **2014**, *14* (11), 6488–6492.
- (37) Valle, G. D.; Hopkins, B.; Ganzer, L.; Stoll, T.; Rahmani, M.; Longhi, S.; Kivshar, Y. S.; De Angelis, C.; Neshev, D. N.; Cerullo, G. Nonlinear Anisotropic Dielectric Metasurfaces for Ultrafast Nanophotonics. *ACS Photonics* **2017**, *4* (9), 2129–2136.
- (38) Koshelev, K.; Tang, Y.; Li, K.; Choi, D.-Y.; Li, G.; Kivshar, Y. Nonlinear Metasurfaces Governed by Bound States in the Continuum. *ACS Photonics* **2019**, *6* (7), 1639–1644.
- (39) Hail, C. U.; Michaeli, L.; Atwater, H. A. Third Harmonic Generation Enhancement and Wavefront Control Using a Local High-Q Metasurface. *Nano Lett.* **2024**, 24 (7), 2257–2263.

- (40) Ooi, K. J. A.; Ng, D. K. T.; Wang, T.; Chee, A. K. L.; Ng, S. K.; Wang, Q.; Ang, L. K.; Agarwal, A. M.; Kimerling, L. C.; Tan, D. T. H. Pushing the Limits of CMOS Optical Parametric Amplifiers with USRN:Si7N3 above the Two-Photon Absorption Edge. *Nat. Commun.* **2017**, 8 (1), No. 13878.
- (41) Choi, J. W.; Sohn, B.-U.; Chen, G. F. R.; Ng, D. K. T.; Tan, D. T. H. Broadband Incoherent Four-Wave Mixing and 27 dB Idler Conversion Efficiency Using Ultra-Silicon Rich Nitride Devices. *Appl. Phys. Lett.* **2018**, *112* (18), No. 181101.
- (42) Xie, H.; Gui, L.; Liu, Y.; Lin, F.; Zhang, Z.; Xu, K. Giant Two-Photon Absorption Response from a Silicon Quasi-BIC Metasurface. *Appl. Phys. Lett.* **2023**, *123* (21), No. 211704.
- (43) Almeida, V. R.; Barrios, C. A.; Panepucci, R. R.; Lipson, M. All-Optical Control of Light on a Silicon Chip. *Nature* **2004**, *431* (7012), 1081–1084.
- (44) Ng, D. K. T.; Wang, Q.; Wang, T.; Ng, S.-K.; Toh, Y.-T.; Lim, K.-P.; Yang, Y.; Tan, D. T. H. Exploring High Refractive Index Silicon-Rich Nitride Films by Low-Temperature Inductively Coupled Plasma Chemical Vapor Deposition and Applications for Integrated Waveguides. ACS Appl. Mater. Interfaces 2015, 7 (39), 21884–21889.
- (45) Son, C.; Peana, S.; Matthiessen, O.; Kryvobok, A.; Senichev, A.; Boltasseva, A.; Shalaev, V. M.; Chekhova, M. Generation of Photon Pairs through Spontaneous Four-Wave Mixing in Subwavelength Nonlinear Films. *Opt. Lett.* **2025**, *50* (13), 4434–4437.
- (46) Noh, J.; Santiago-Cruz, T.; Sultanov, V.; Doiron, C. F.; Gennaro, S. D.; Chekhova, M. V.; Brener, I. Quantum Pair Generation in Nonlinear Metasurfaces with Mixed and Pure Photon Polarizations. *Nano Lett.* **2024**, *24* (48), 15356–15362.
- (47) Liu, T.; Qin, M.; Feng, S.; Tu, X.; Guo, T.; Wu, F.; Xiao, S. Efficient Photon-Pair Generation Empowered by Dual Quasibound States in the Continuum. *Phys. Rev. B* **2024**, *109* (15), No. 155424.
- (48) Minkov, M.; Williamson, I. A. D.; Andreani, L. C.; Gerace, D.; Lou, B.; Song, A. Y.; Hughes, T. W.; Fan, S. Inverse Design of Photonic Crystals through Automatic Differentiation. *ACS Photonics* **2020**, *7* (7), 1729–1741.
- (49) Zanotti, S.; Minkov, M.; Nigro, D.; Gerace, D.; Fan, S.; Andreani, L. C. Legume: A Free Implementation of the Guided-Mode Expansion Method for Photonic Crystal Slabs. *Comput. Phys. Commun.* **2024**, 304, No. 109286.

